

Faceted particles formed by the frustrated packing of anisotropic colloids on curved surfaces

Naiyin Yu and Michael F. Hagan*

Martin Fisher School of Physics, Brandeis University, Waltham, MA, USA.

We use computer simulations and simple theoretical models to analyze the morphologies that result when rod-like particles end-attach onto a curved surface, creating a finite-thickness monolayer aligned with the surface normal. This geometry leads to two forms of frustration, one associated with the incompatibility of hexagonal order on surfaces with Gaussian curvature, and the second reflecting the deformation of a layer with finite thickness on a surface with non-zero mean curvature. We show that the latter effect leads to a faceting mechanism. Above threshold values of the inter-particle attraction strength and surface mean curvature, the adsorbed layer undergoes a transition from orientational disorder to an ordered state that is demarcated by reproducible patterns of line defects. The number of facets is controlled by the competition between line defect energy and intra-facet strain. Tuning control parameters thus leads to a rich variety of morphologies, including icosahedral particles and irregular polyhedra. In addition to suggesting a new strategy for the synthesis of aspherical particles with tunable symmetries, our results may shed light on recent experiments in which rod-like HIV GAG proteins assemble around nanoscale particles.

The formation of crystalline or liquid crystalline order on curved surfaces is frustrated, resulting in topological defects. For example, while the densest packing of disks is a six-fold coordinated hexagonal lattice which perfectly tiles the plane, placing such a lattice on a spherical surface requires at minimum 12 five-fold coordinated disks [1, 2]. Similarly, forming a nematic phase on a spherical surface requires defects with net topological charge +2 [3, 4]. Despite intense theoretical and experimental research into ordering on curved surfaces for more than 100 years (*e.g.* [1, 2, 4–27]), studies have focused on systems in which molecules are confined within the local tangent surface.

Here, we study the coupling between particle shape and curvature that arises when anisotropic (rod-like) particles tend to align along the surface normal. Our model is motivated by recent experiments on the assembly of rod-like HIV GAG proteins assembling around spherical nanoparticles [28], and the discovery that rodlike molecules with interparticle attractions can form stable monolayers [29–31]. We find that this geometry leads to two forms of frustration, one familiar from the packing of disks on a sphere, and the second reflecting the strain required to deform a layer of finite thickness on a curved surface. Frustrated sphere packing is an effect of intrinsic geometry (metric in origin) and thus requires non-zero Gaussian curvature. In contrast, the strain associated with layer thickness arises due to coupling between bend and splay and depends on extrinsic (mean) curvature. Thus, the latter effect occurs even in cylindrical geometries with zero Gaussian curvature. The interplay between frustrations of extrinsic and intrinsic origin leads to a rich variety of faceted shapes, including those with icosahedral symmetry and other polyhedra with lower symmetry, whose features can be readily tuned by con-

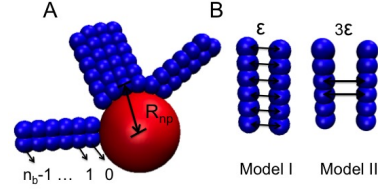


FIG. 1. (Color online) Schematic of the models. **(A)** Rods are modeled as rigid strings of beads. Examples are shown with $n_b = 6$ beads. The bottom bead in each rod is attracted to the nanoparticle. The distance between the centers of the nanoparticle and the first bead of an adsorbed rod is denoted R_{np} . **(B)** Two inter-rod potentials are considered. In Model I, bead-bead attractions are distributed uniformly along the rods; in Model II, interactions occur only between the middle beads.

trolling template size and inter-particle interactions. In addition to elucidating how multiple forms of packing constraints can conspire to modulate order, our findings identify a new design strategy for synthesizing particles with aspherical shapes. Such particles are of great interest in the nanomaterials and colloidal communities, since they can assemble into an extraordinary range of structures (*e.g.* [32–42]). Previous studies have shown that flexible ligands on isolated or clustered nanoparticles can order to form spherically asymmetric coatings [34, 43–74]. The current work demonstrates that rigid ligands can also order to form diverse morphologies that, despite their complexity, can be predicted from simple statistical mechanics arguments.

Model and methods. Our system contains a rigid nanosphere with radius $R_{np} - \sigma_b/2$ and N_{rods} rigid rods comprised of n_b beads separated by a distance equal to their diameter σ_b . Rods dynamically adsorb end-first onto the nanosphere, and are driven by lateral rod-rod interactions to form a layer aligned with the local nanosphere normal (Fig. 1). Beads from differ-

* hagan@brandeis.edu

ent rods experience excluded volume interactions represented by a repulsive Lennard-Jones potential $V_{\text{LJ}}(r; \sigma_b)$, Eq. 1. In addition, beads with the same index (counting from $n = 0$ at the rod bottom) experience attractive interactions represented by a Morse potential $V_{\text{morse}}(r; \varepsilon_n, \sigma_b, \alpha = 7.5\sigma_b)$, Eq. 2, with ε_n as the well-depth for the attraction between beads with index n :

$$V_{\text{LJ}}(r; s) = \left[\left(\frac{s}{r} \right)^{12} - 1 \right] H(s - r) \quad (1)$$

$$V_{\text{morse}}(r; \varepsilon, s, \alpha) = \varepsilon \left(e^{-2\alpha(r-s)} - 2e^{-\alpha(r-s)} \right) \times H(1.5s - r) - V_{\text{shift}} \quad (2)$$

where $H(x)$ is the Heaviside function and $V_{\text{shift}} \approx -0.001$. We consider two distributions of attractions along the rods (Fig. 1): (Model I) uniform attractions with $\varepsilon_n = \varepsilon \forall n$, and (Model II) attractions occur for the middle 1/3 of beads, with strength $\varepsilon_n = 3\varepsilon$.

All beads experience excluded volume interactions with the nanoparticle given by $V_{\text{LJ}}(r; R_{\text{np}})$ with R_{np} the center-to-center distance between the nanosphere and a bead on its surface. In addition, the first bead in each rod ($n = 0$) is attracted to the nanoparticle by $V_{\text{morse}}(r; \varepsilon_{\text{np}}, R_{\text{np}}, \alpha = 15)$ with $\varepsilon_{\text{np}} = 20k_{\text{B}}T$ parameterizing the rod-nanoparticle interaction strength.

We performed Brownian dynamics simulations with HOOMD [75–77]. Energies and lengths are presented in units of the thermal energy $k_{\text{B}}T$ and the bead diameter σ_b respectively. For each simulation the nanoparticle was fixed in the center of the simulation box, and initial rod configurations and orientations were chosen randomly, except excluded volume overlaps were not allowed. Periodic boundary conditions were employed. The system was first equilibrated for 5×10^6 steps with attractions disabled ($\varepsilon = \varepsilon_{\text{np}} = 0$). Simulations were then integrated for at least 2×10^9 steps, with time step 10^{-3} .

Cylindrical model in 2D. To consider a case with only mean curvature, we also analyze a simplified two-dimensional (2D) system, where rods are end-attached onto the outside of a circular boundary (*i.e.* a 2D slice of a cylindrical nanoparticle). For simplicity, we do not simulate the dynamics of rod adsorption onto the cylinder. We consider a grafting density equal to close packing on the surface of the cylinder, $N_{\text{rods}} = \pi / \sin^{-1}(\sigma_b / 2R_{\text{np}})$, so the position of each rod end bead is fixed but rods can rotate.

Results. Except where mentioned otherwise, we focus on the 3D system. All simulations resulted in rods strongly end-adsorbed to the nanoparticle to yield a dense layer. The bottom beads, which are attracted to the nanoparticle, form local hexagonal order punctuated by 12 five-fold defects arranged with icosahedral symmetry as observed for the packing of spheres on a spherical surface [5, 10].

For weak inter-rod interactions (small ε), rod orientations are random, leading to disordered arrangements of beads in the layers above the surface. Above a threshold strength ε^* , we observe a transition to an ordered

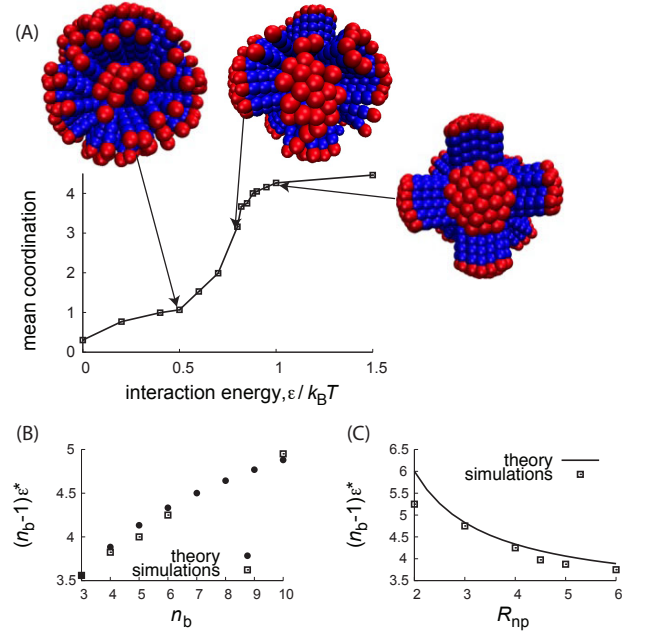


FIG. 2. (Color online) (A) The mean coordination number of beads in the outermost layer is shown as a function of the bead interaction strength ε for aspect ratio $n_b = 6$ and nanoparticle radius $R_{\text{np}} = 4$. Snapshots of final simulation structures are shown for indicated values of ε . To aid visibility, the outermost beads are colored red whereas others are colored blue. (B), (C) The transition interaction strength ε^* from simulations and the theory [78] is shown as a function of (A) n_b for $R_{\text{np}} = 4$ and (B) R_{np} for $n_b = 6$. We determine ε^* as the smallest interaction strength at which the number of 6-fold coordinated rods exceeds the number with 5-fold coordination.

layer with most rods parallel to their nearest neighbors (Fig. 2). The value of ε^* is determined by the competition between the orientational entropy of rods in the disordered state and the attractive interactions of parallel rods. We approximately calculate how this competition depends on R_{np} and n_b in [78]. The results of this calculation are compared to simulation results in Fig. 2B,C.

Due to the nanoparticle curvature, rods cannot all maintain parallel orientations and fixed interaction distances with their neighbors. Thus, the system undergoes a spontaneous symmetry breaking in which the surface is demarcated by line defects which form a polyhedron that inscribes the nanoparticle surface. Within each ‘face’ rods are roughly parallel and arranged with hexagonal close packing. Interestingly, the defect lines do not necessarily form a regular polyhedron. For example, with $R_{\text{np}} = 4$, at all simulated aspect ratios, we observed approximately nine faces, with individual faces differing in size and number of edges. The number of faces increases slowly with R_{np} (Fig. 3).

Simulations on the 2D cylinder system showed similar behavior. In the limit of hard spheres and a short-range attractive interaction, $\alpha \rightarrow \infty$, the energy minimizing configurations of this system can be

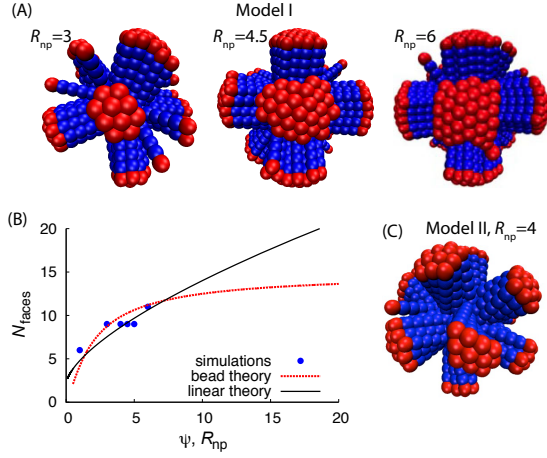


FIG. 3. (Color online) (A) Simulation snapshots at indicated spherical nanoparticle sizes for Model I interactions. (B) The number of faces in the spherical geometry with Model I interactions as a function of R_{np} for the simulations (points) and the theory accounting for bead intercalation (Eq. (3), red dotted line), and as a function of ψ for the linear tilt theory (Eqs. (4), black line). (C) Simulation snapshot for Model II interactions with $R_{np}=4$, showing 12 faces. Other parameters are $n_b = 6$ and $\varepsilon/k_B T = 1$ for (A)-(C).

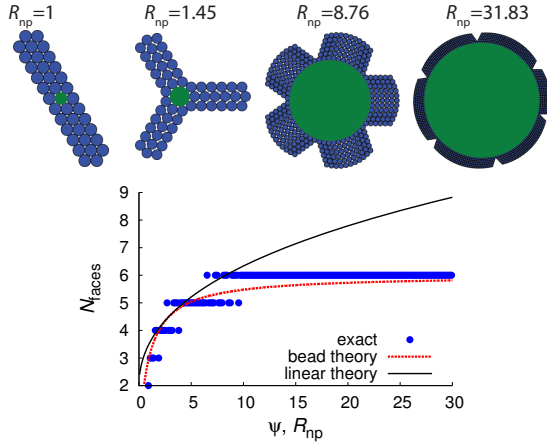


FIG. 4. (Color online) The number of faces in a circular geometry is plotted as a function of R_{np} for results from exact energy minimizing configurations (points) and the sphere intercalation theory (red dotted line), and as a function of ψ for the theory (Eqs. (5), line). Snapshots of energy minimizing configurations at several values of R_{np} are shown on top, with rod beads colored blue and the nanoparticle in green.

calculated exactly. The number of faces is given by $N_{\text{faces}}^{\text{exact}} = \lceil N_{\text{rods}} / [2 + N_{\text{rods}}/6] \rceil$. The dependence of $N_{\text{faces}}^{\text{exact}}$ on nanoparticle radius and example configurations are shown in Fig. 4.

Factors that determine the number of faces. It is well known that incompatibility between a materials preferred local packing geometry and long-range order can lead to defect-stabilized phases (*e.g.* Frank-Kasper phases, blue phases, and twist-grain-boundary phases), in which

finite-sized unfrustrated domains are separated by regions of broken short-range order (defects) [2]. In our simulations, we observe an analog of this behavior on finite nanoparticle surfaces. The resulting defect geometries can be understood from the following simple models. While the packing of flexible ligands in curved layers has been analyzed [68], different considerations are required for the rodlike particles considered here.

We consider a face (patch of nearly parallel, hexagonally ordered rods) whose orientations are aligned with the sphere normal at the patch center, which we define as the z -axis. Away from the center of the face, the nanoparticle curvature forces rods out of register. For the rod excluded-volume geometry that we consider (a chain of spheres), this displacement can be accommodated by intercalation of neighboring rods until the patch extends along the surface to an angle bounded by

$$\theta_d \approx \pi/6 + 0.5\sigma_b/R_{np}, \quad (3)$$

where the second factor accounts for rod granularity. Growth of the patch beyond θ_d would lead to a large strain energy which increases with patch size. This is avoided by terminating the patch and commencing a new one with a different rod orientation. The two patches are thus separated by a line defect. The number of faces N_{faces} can then be estimated from the fraction of the nanoparticle surface occupied by a single patch, giving $N_{\text{faces}} = 2/(1 - \cos \theta_d)$ for spherical nanoparticles and $N_{\text{faces}} = \pi/\theta_d$ for cylinders. These relationships qualitatively agree with the numbers of faces observed in simulations (Figs. 3 and 4).

While the model just described depends on the local packing geometry of our rods, the effect is general. To show this, we consider deposition on a spherical or cylindrical substrate of a film with sufficient thickness δ that shear or tilt deformations correspond to lower energy than bending. For simplicity, we consider a linear tilt modulus G (although our simulated rod monolayer has a highly nonlinear stress-strain relationship).

We then consider a circular domain of such a material as defined above. As the domain extends across the surface by an angle θ_d , the material undergoes a strain along \hat{z} given by $\gamma(\theta) = \tan \theta$. The domain boundary gives rise to an interfacial energy characterized by a line tension σ , which we expect to be proportional to the film thickness δ . The total energy density U_{tot} is given by integrating the strain energy over the domain area, and summing over the number of domains N_{faces} :

$$\frac{U_{\text{sphere}}(\theta_d)}{4\pi R_{np}^2 \delta G} = \frac{N_{\text{faces}}(\theta_d)}{2} [(\cos \theta_d + \sec \theta_d - 2) + \psi^{-1} \sin \theta_d] \quad (4)$$

with $\psi \equiv R_{np}\delta G/\sigma$ the dimensionless ratio between shear modulus and line tension. The term in parentheses on the right-hand side of Eq. (4) gives the strain energy, the next term is the interfacial energy, and we neglect contributions from the 12 disclinations required by the

spherical geometry [79]. Because the tilt modulus and interfacial energy are both dictated by the strength of molecular interactions, we expect the line tension to be proportional to the film thickness δ and hence the quantity $\psi \propto R_{\text{np}}/\sigma_b$ with σ_b the molecular spacing.

A similar analysis for a cylinder with radius R_{np} and length L yields

$$\frac{U_{\text{cyl}}(\theta_d)}{2\pi R_{\text{np}} L \delta G} = \frac{1}{2\theta_d} [(\tan \theta_d - \theta_d) + \psi^{-1}] \quad (5)$$

The size and number of domains θ_d and N_{faces} are obtained by minimizing Eq. (4) or (5). As shown in Fig. 3, the linear theories qualitatively describe the simulation results, except that the predicted number of faces monotonically increases with R_{np} . In the simulated systems, the bead intercalation cuts off N_{faces} at about 15 or 6 for spheres or cylinders respectively. In both geometries the number of domains approaches two as ψ approaches zero (corresponding to small particle size or small tilt modulus). In this limit, the material in each hemisphere aligns with the z-axis with an equatorial defect between the two domains, resembling structures observed in simulations of flexible alkanes on gold nanoparticles [68, 69]. The similarity between the results on spherical and curvature substrates emphasizes that the frustration associated with depositing a thick film on a curved substrate is correlated to mean curvature, in contrast to the frustration of packing discs on a spherical surface associated with Gaussian curvature.

For sufficiently large nanoparticles the system will enter the thin film limit, with bending deformations lower in energy than tilt. (While U_{sphere} and U_{cyl} monotonically increase with R_{np} , the bending energy of an elastic layer is independent of R_{np} in a spherical geometry and decreases as $\sim R_{\text{np}}^{-1}$ for a cylinder.) We thus anticipate a critical nanoparticle size above which faceting does not occur, given by $R_{\text{np}}^* \sim \delta \sigma_b \alpha$ with α^{-1} the width of the interparticle potential.

Intra-bundle twist leads to another mechanism of frustration. While the interactions along the rods are uniform in the simulations described to this point (Model I, Fig. 1), simulations with interactions were confined to the middle two beads (Model II) resulted in an approximately regular dodecahedron (Fig. 3C). The 12-face morphology appears to arise because, with interactions between only the middle 2 beads, the rods form twisted bundles. Inter-filament twisting provides another form of frustration which can limit the lateral growth of bundles [80–83], which likely couples with the curvature-induced frustration to decrease the critical face size. Importantly, upon switching the interaction to Model I, the 12-face structure reconfigured to the 9-face structure. Switching back to Model II then caused reconfiguration to the 12-face structure (Fig. S1 [78]). Since these reconfigurations require extensive morphological changes and numbers of adsorbed rods (Figs. S1, S2 [78]), these reversible changes suggest that the structures correspond to equilibrium morphologies.

In conclusion, our simulations and simple theoretical models demonstrate that the geometric frustration intrinsic to assembling anisotropic particles on curved surfaces leads to diverse equilibrium morphologies. While the specific number of faces obtained at a given parameter set depends on the details of the interparticle interaction potential, a simple model based on a generic linear stress-strain relationship predicts qualitatively similar behaviors. Thus, it should be possible to generate polyhedral morphologies using a wide range of particle shapes and interactions. Extending our model to describe other interparticle interactions or substrate geometries would enable designing alternative assembly morphologies. Controlling the strength of interparticle interactions (e.g. by temperature or depletant concentration) enables reversible switching between ordered, faceted morphologies and disordered structures. Moreover, by changing the form of inter-particle potentials, it is possible to obtain highly symmetric structures (e.g. a dodecahedron) or asymmetric structures (e.g. the 9-face polyhedron).

Our model was particularly motivated by two experimental systems. First, Dogic and coworkers [29] showed that a suspension of rodlike viruses and non-adsorbing polymer form 2D colloidal membranes, comprised of one rod-length thick monolayers of aligned rods. Deposition of such a monolayer onto a colloidal particle could be driven by depletion interactions [84] or complementary functionalization of rod ends and nanoparticle surfaces. It would be interesting to observe the morphologies of such assemblages as a function of nanoparticle size, depletant concentration, and depletant size. Second, cryoEM micrographs of HIV GAG proteins assembled around functionalized nanoparticles exhibit extensive scars that resemble features of the line defects and disorder observed in our simulations (Fig. S2 [78]). However, we note that the GAG protein assembles with a preferred curvature in the absence of a spherical template, in contrast to the rod-like particles considered here. The physics described here will be most relevant to cases in which the nanoparticle radius is small in comparison to the cone angle. For larger nanoparticles, GAG proteins could be better represented by conical particles (e.g. [85]). For cone angles which are commensurate with the nanoparticle radius, the frustration resulting from mean curvature would be avoided, and we would expect similar morphologies to those observed for packing of discs on a sphere [85].

ACKNOWLEDGMENTS

We acknowledge Greg Grason for insightful comments on the manuscript and support from NIGMS R01GM108021 and the Brandeis University NSF MRSEC, DMR-1420382. Computational resources were provided by the NSF through XSEDE computing resources (Trestles and Stampede) and the Brandeis HPCC which is partially supported by the Brandeis MRSEC. MFH acknowledges the Aspen Center for Physics (NSF 1066293)

and Kavli Institute for Theoretical Physics (NSF PHY11-

25915) for support during this work.

-
- [1] J. J. Thompson, *Philos. Mag.* **7**, 237 (1904).
 - [2] M. Kleman, *Adv. Phys.* **38**, 605 (1989).
 - [3] H. Poincaré, *Journal de mathématiques pures et appliquées* **4**, 167 (1885).
 - [4] N. D. Mermin, *Rev. Mod. Phys.* **51**, 591 (1979).
 - [5] M. Bowick, D. Nelson, and A. Travesset, *Phys. Rev. B* **62**, 8738 (2000).
 - [6] M. Bowick, A. Cacciuto, D. Nelson, and A. Travesset, *Phys. Rev. Lett.* **89**, 185502 (2002).
 - [7] D. L. D. Caspar and A. Klug, *Cold Spring Harbor Symp. Quant. Biol.* **27**, 1 (1962).
 - [8] D. Nelson, *Defects and Geometry in Condensed Matter Physics* (Cambridge University Press, 2002).
 - [9] E. Altschuler, T. Williams, E. Ratner, R. Tipton, R. Stong, F. Dowla, and F. Wooten, *Phys. Rev. Lett.* **78**, 2681 (1997).
 - [10] A. Bausch, M. Bowick, A. Cacciuto, A. Dinsmore, M. Hsu, D. Nelson, M. Nikolaides, A. Travesset, and D. Weitz, *Science* **299**, 1716 (2003).
 - [11] W. T. M. Irvine, V. Vitelli, and P. M. Chaikin, *Nature* **468**, 947 (2010).
 - [12] A. Fernández-Nieves, V. Vitelli, A. S. Utada, D. R. Link, M. Márquez, D. R. Nelson, and D. A. Weitz, *Phys. Rev. Lett.* **99**, 157801 (2007).
 - [13] T. Lopez-Leon, A. Fernandez-Nieves, M. Nobili, and C. Blanc, *J. Phys.: Condens. Matter* **24** (2012).
 - [14] T. Lopez-Leon, A. Fernandez-Nieves, M. Nobili, and C. Blanc, *Phys. Rev. Lett.* **106** (2011).
 - [15] H. L. Liang, S. Schymura, P. Rudquist, and J. Lagerwall, *Phys. Rev. Lett.* **106** (2011).
 - [16] H. L. Liang, J. Noh, R. Zentel, P. Rudquist, and J. P. F. Lagerwall, *Phil. Trans. R. Soc. A* **371** (2013).
 - [17] T. Lopez-Leon, V. Koning, K. B. S. Devaiah, V. Vitelli, and A. Fernandez-Nieves, *Nat. Phys.* **7**, 391 (2011).
 - [18] G. Meng, J. Paulose, D. R. Nelson, and V. N. Manoharan, *Science* **343**, 634 (2014).
 - [19] H. Kusumaatmaja and D. J. Wales, *Phys. Rev. Lett.* **110** (2013).
 - [20] W. T. M. Irvine and V. Vitelli, *Soft Matter* **8**, 10123 (2012).
 - [21] W. T. M. Irvine, M. J. Bowick, and P. M. Chaikin, *Nat. Mater.* **11**, 948 (2012).
 - [22] G. M. Grason and B. Davidovitch, *Proc. Natl. Acad. Sci. U. S. A.* **110**, 12893 (2013).
 - [23] A. Azadi and G. M. Grason, *Phys. Rev. Lett.* **112**, 225502 (2014).
 - [24] B. L. Mbang, G. M. Grason, and C. D. Santangelo, *Phys. Rev. Lett.* **108**, 017801 (2012).
 - [25] I. R. Bruss and G. M. Grason, *Proc. Natl. Acad. Sci. U. S. A.* **109**, 10781 (2012).
 - [26] G. M. Grason, *Soft Matter* **9**, 6761 (2013).
 - [27] G. M. Grason, *Rev. Mod. Phys.* **87**, 401 (2015).
 - [28] N. L. Goicochea, S. A. K. Datta, M. Ayaluru, C. Kao, A. Rein, and B. Dagnea, *J. Mol. Biol.* **410**, 667 (2011).
 - [29] E. Barry and Z. Dogic, *Proc. Nat. Acad. Sci.* **107**, 10348 (2010).
 - [30] J. L. Baker, A. Widmer-Cooper, M. F. Toney, P. L. Geissler, and A. P. Alivisatos, *Nano Lett.* **10**, 195 (2010).
 - [31] Y. Yang, E. Barry, Z. Dogic, and M. F. Hagan, *Soft Matter* **8**, 707 (2012).
 - [32] G. van Anders, N. K. Ahmed, R. Smith, M. Engel, and S. C. Glotzer, *Acs Nano* **8**, 931 (2014).
 - [33] S. C. Glotzer and M. J. Solomon, *Nat. Mater.* **6**, 557 (2007).
 - [34] C. Singh, P. K. Ghorai, M. A. Horsch, A. M. Jackson, R. G. Larson, F. Stellacci, and S. C. Glotzer, *Phys. Rev. Lett.* **99** (2007).
 - [35] E. Duguet, A. Desert, A. Perro, and S. Ravaine, *Chem. Soc. Rev.* **40**, 941 (2011).
 - [36] S. Sacanna, W. T. M. Irvine, P. M. Chaikin, and D. J. Pine, *Nature* **464**, 575 (2010).
 - [37] G. R. Yi, D. J. Pine, and S. Sacanna, *J. Phys.: Condens. Matter* **25** (2013).
 - [38] Y. Yang, L. Gao, G. P. Lopez, and B. B. Yellen, *Acs Nano* **7**, 2705 (2013).
 - [39] S. Whitelam, I. Tamblyn, T. K. Haxton, M. B. Wieland, N. R. Champness, J. P. Garrahan, and P. H. Beton, *Phys. Rev. X* **4** (2014).
 - [40] Y. F. Wang, Y. Wang, D. R. Breed, V. N. Manoharan, L. Feng, A. D. Hollingsworth, M. Weck, and D. J. Pine, *Nature* **491**, 51 (2012).
 - [41] Y. Wang, Y. F. Wang, X. L. Zheng, G. R. Yi, S. Sacanna, D. J. Pine, and M. Weck, *J. Am. Chem. Soc.* **136**, 6866 (2014).
 - [42] A. Walther and A. H. E. Muller, *Chem. Rev.* **113**, 5194 (2013).
 - [43] W. L. Miller, B. Bozorgui, K. Klymko, and A. Cacciuto, *J. Chem. Phys.* **135** (2011).
 - [44] K. Larson-Smith and D. C. Pozzo, *Soft Matter* **7**, 5339 (2011).
 - [45] K. M. Harkness, A. Balinski, J. A. McLean, and D. E. Cliffl, *Angew. Chem., Int. Ed.* **50**, 10554 (2011).
 - [46] P. K. Ghorai and S. C. Glotzer, *J. Phys. Chem. C* **114**, 19182 (2010).
 - [47] P. K. Ghorai and S. C. Glotzer, *J. Phys. Chem. C* **111**, 15857 (2007).
 - [48] C. Gentilini and L. Pasquato, *J. Mater. Chem.* **20**, 1403 (2010).
 - [49] C. Gentilini, P. Franchi, E. Mileo, S. Polizzi, M. Lucarini, and L. Pasquato, *Angew. Chem., Int. Ed.* **48**, 3060 (2009).
 - [50] Y. Cesbron, C. P. Shaw, J. P. Birchall, P. Free, and R. Levy, *Small* **8**, 3714 (2012).
 - [51] R. P. Carney, G. A. DeVries, C. Dubois, H. Kim, J. Y. Kim, C. Singh, P. K. Ghorai, J. B. Tracy, R. L. Stiles, R. W. Murray, S. C. Glotzer, and F. Stellacci, *J. Am. Chem. Soc.* **130**, 798 (2008).
 - [52] M. Yu and F. Stellacci, *Small* **8**, 3720 (2012).
 - [53] R. C. Van Lehn, P. U. Atukorale, R. P. Carney, Y. S. Yang, F. Stellacci, D. J. Irvine, and A. Alexander-Katz, *Nano Lett.* **13**, 4060 (2013).
 - [54] C. Tung and A. Cacciuto, *J. Chem. Phys.* **139** (2013).
 - [55] S. Tawfick, M. De Volder, D. Copic, S. J. Park, C. R. Oliver, E. S. Polsen, M. J. Roberts, and A. J. Hart, *Advanced Materials* **24**, 1628 (2012).
 - [56] A. Stewart, S. Zheng, M. R. McCourt, and S. E. J. Bell,

- [Acs Nano](#) **6**, 3718 (2012).
- [57] C. Singh, Y. Hu, B. P. Khanal, E. R. Zubarev, F. Stellacci, and S. C. Glotzer, [Nanoscale](#) **3**, 3244 (2011).
 - [58] P. Possocco, C. Gentilini, S. Bidoggia, A. Pace, P. Franchi, M. Lucarini, M. Fermeglia, S. Pricl, and L. Pasquato, [Acs Nano](#) **6**, 7243 (2012).
 - [59] I. C. Pons-Siepermann and S. C. Glotzer, [Soft Matter](#) **8**, 6226 (2012).
 - [60] I. C. Pons-Siepermann and S. C. Glotzer, [Acs Nano](#) **6**, 3919 (2012).
 - [61] R. Sknepnek, G. Vernizzi, and M. O. de la Cruz, [Soft Matter](#) **8**, 636 (2012).
 - [62] V. Jadhao, C. K. Thomas, and M. O. de la Cruz, [Proc. Natl. Acad. Sci. U. S. A.](#) **111**, 12673 (2014).
 - [63] G. Vernizzi and M. O. de la Cruz, [Proc. Natl. Acad. Sci. U. S. A.](#) **104**, 18382 (2007).
 - [64] A. Santos, J. A. Millan, and S. C. Glotzer, [Nanoscale](#) **4**, 2640 (2012).
 - [65] A. Badia, L. Cuccia, L. Demers, F. Morin, and R. B. Lennox, [J. Am. Chem. Soc.](#) **119**, 2682 (1997).
 - [66] M. T. Frederick, J. L. Achtyl, K. E. Knowles, E. A. Weiss, and F. M. Geiger, [J. Am. Chem. Soc.](#) **133**, 7476 (2011).
 - [67] U. Landman and W. D. Luedtke, [Faraday Discuss.](#) **125**, 1 (2004).
 - [68] J. M. D. Lane and G. S. Grest, [Phys. Rev. Lett.](#) **104**, 235501 (2010).
 - [69] W. D. Luedtke and U. Landman, [J. Phys. Chem. B](#) **102**, 6566 (1998).
 - [70] W. D. Luedtke and U. Landman, [J. Phys. Chem.](#) **100**, 13323 (1996).
 - [71] A. Widmer-Cooper and P. Geissler, [Nano Lett.](#) **14**, 57 (2014).
 - [72] Z. Yang, X. N. Yang, Z. J. Xu, and N. N. Yang, [J. Chem. Phys.](#) **133**, 094702 (2010).
 - [73] M. Asai, A. Cacciuto, and S. K. Kumar, [Soft Matter](#) **11**, 793 (2015).
 - [74] A. H. R. Koch, G. Leveque, S. Harms, K. Jaskiewicz, M. Bernhardt, A. Henkel, C. Sonnichsen, K. Landfester, and G. Fytas, [Nano Lett.](#) **14**, 4138 (2014).
 - [75] J. A. Anderson, C. D. Lorenz, and A. Travesset, [J. Comput. Phys.](#) **227**, 5342 (2008).
 - [76] T. D. Nguyen, C. L. Phillips, J. A. Anderson, and S. C. Glotzer, [Comput. Phys. Commun.](#) **182**, 2307 (2011).
 - [77] D. N. LeBard, B. G. Levine, P. Mertmann, S. A. Barr, A. Jusufi, S. Sanders, M. L. Klein, and A. Z. Panagiotopoulos, [Soft Matter](#) **8**, 2385 (2012).
 - [78] See Supplemental Material at [URL will be inserted by publisher].
 - [79] One might also consider rod-like particles interacting through depletion interactions, such as in the colloidal membranes system studied by Barry et al. [29]. Since the depletion interaction depends only on overlapping occluded volume rather than pairwise interactions between specific molecular groups, tilting affects the interaction between neighboring rods only near their ends. However, since neighboring rods cannot overlap, tilting reduces the aerial density by a factor $\rho(\theta) \propto 1 - \cos(\theta)$. Accounting for this density reduction leads to a similar dependence of N_{faces} on R_{np} as in Eq. (4).
 - [80] G. M. Grason and R. F. Bruinsma, [Phys. Rev. Lett.](#) **99**, 098101 (2007).
 - [81] Y. Yang, R. Meyer, and M. F. Hagan, [Phys. Rev. Lett.](#) **104**, 258102 (2010).
 - [82] G. M. Grason, [Phys. Rev. Lett.](#) **101**, 105702 (2008).
 - [83] G. M. Grason, [Phys. Rev. E](#) **79**, 041919 (2009).
 - [84] S. Asakura and F. Oosawa, [J. Chem. Phys.](#) **22**, 1255 (1954).
 - [85] T. Chen, Z. L. Zhang, and S. C. Glotzer, [Proc. Natl. Acad. Sci. U. S. A.](#) **104**, 717 (2007).

Faceted particles formed by the frustrated packing of anisotropic colloids on curved surfaces

Supplementary Materials

Naiyin Yu and Michael F. Hagan*

Martin Fisher School of Physics, Brandeis University, Waltham, MA, USA.

In this supplement, we present a calculation for how the order/disorder transition interaction strength ϵ^* depends on particle size and rod aspect ratio, as well as additional figures.

DISORDERED TO ORDERED TRANSITION

The interaction strength ϵ^* required to form polyhedral particles is determined by the competition between the orientational entropy of rods in the disordered state and the attractive interactions of rods in the polyhedral state. We quantify this competition as follows. The orientational free energy of a rod in the disordered state is given by $f_{\text{free}}/k_B T = \log 2$, where we neglect excluded volume with neighboring rods, assume that the nanoparticle surface restricts rod orientations to a solid angle of 2π , and that rods have free orientations in the reference state. To calculate the free energy of rods within a polyhedral face, we first estimate the binding free energy between two neighboring rods:

$$\beta f_b(\epsilon, n_b) = -\log[q_{\text{rod}}(\epsilon, n_b)/4\pi]$$

$$q_{\text{rod}}(\epsilon, n_b) = \frac{2\pi}{\sigma_b^2 \beta V''_{\text{morse}} \sum_{n=1}^{n_b-1} n^2} \exp[(n_b - 1)\epsilon/k_B T]$$
(S1)

with q_{rod} the partition function for the interaction between two rods integrated over angular fluctuations within the bound state, $V''_{\text{morse}} = 2\epsilon\alpha^2$ is the second derivative of the Morse potential evaluated at its minimum, and we have expanded the interaction potential to second-order. Notice that the relevant rod-rod interaction strength parameter is $(n_b - 1)\epsilon$, since the interaction between the innermost beads of neighboring rods is independent of their orientations.

Each interior rod within a polyhedral face interacts with six neighbors, whereas those on the perimeter interact with on average 3.5 neighbors. We therefore approximate the binding free energy of interior rods as $f_b(3\epsilon)$, accounting for double counting, and perimeter rods as $f_b(3.5\epsilon/2)$. For a face with n_{rod} rods, the fraction of rods on the perimeter can be approximated as

$$f_{\text{perim}} = 2(\pi/N_{\text{rods}}\rho_{\text{HCP}})^{1/2}$$
(S2)

$$n_{\text{rod}} = 4\pi R_{\text{np}}^2 \rho_{\text{HCP}} / \sigma_b^2 N_{\text{faces}}(R_{\text{np}})$$
(S3)

with $\rho_{\text{HCP}} = 2/\sqrt{3}$ and $N_{\text{faces}}(R_{\text{np}})$ the number of faces as a function of nanoparticle size, given by Eq.(3) and

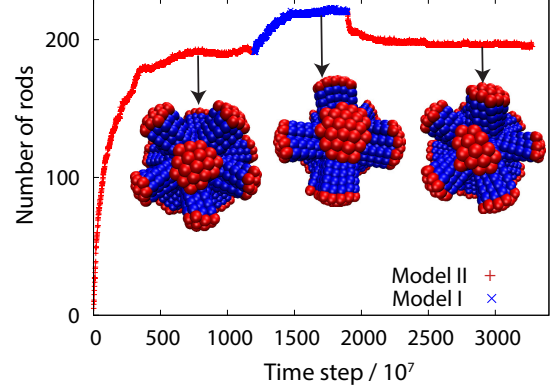


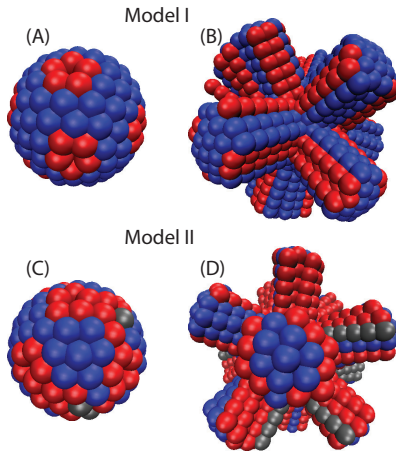
FIG. S1. Reversible transitions between morphologies. The number of rods adsorbed on the nanoparticle is shown as a function of simulation time step, for a simulation starting with the Model II potential (+ symbols), switching to the Model I potential (x symbols), and returning to the Model II potential. Snapshots are shown from indicated time steps, with respectively 12, 9, and 12 faces.

$N_{\text{faces}} = 2/(1 - \cos \theta_d)$ (main text). The free energy per rod within a face is then given by

$$\Delta f(\epsilon, n_b, R_{\text{np}})/k_B T = (1 - f_{\text{perim}}) f_b(3\epsilon, n_b) + f_{\text{perim}} f_b(1.75\epsilon, n_b)$$
(S4)

Finally, the value of the transition ϵ^* is determined by $\Delta f(\epsilon^*, n_b, R_{\text{np}}) = f_{\text{free}}$. The calculated transition values are compared to simulation results in main text Fig. 2 as functions of n_b and R_{np} . We see that the theoretical prediction agrees closely with the simulation results except at small R_{np} , where the continuum limit breaks down.

ADDITIONAL FIGURES



* hagan@brandeis.edu

FIG. S2. Relationship between inner layer disclinations and outer layer fissures. For each model (model I, top panel and model II, bottom panel), the coordination number of spheres in the inner layer **(A),(C)** is shown next to an image displaying all layers **(B),(D)**, with rods colored by their coordination number in the inner layer. The nanoparticle radius is $R_{np}=4$, the interaction energy is $\epsilon=1$, and coordination numbers are indicated as: blue=6, red=5, grey=4.